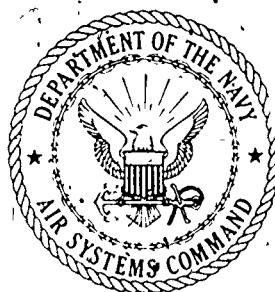69 3234

A METHOD OF COMPUTING HELICOPTER VORTEX WAKE DISTORTION

M.P. Scully

Massachusetts Institute of Technology
Aeroelastic and Structures Research Laboratory
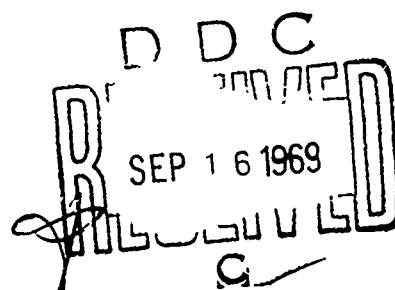
JUNE 1967

ASRL TR 138-1

A METHOD OF COMPUTING HELICOPTER VORTEX
WAKE DISTORTION

M.P. Scully

MASSACHUSETTS INSTITUTE OF TECHNOLOGY
AEROELASTIC AND STRUCTURES RESEARCH LABORATORY

June 1967

Distribution of this report is unlimited

DDC

SEP 1 6 1969

for the

SUMMARY

A method for computing the geometry of the tip vortex of a helicopter rotor in steady, forward flight, including the distortion due to the velocities induced by the vortex wake, has been developed. The relative importance of various parameters and approximations used by this method has been evaluated for one test case, including comparison with experimental results obtained from a flow visualization study.

TABLE OF CONTENTS

List of Figures

NOMENCLATURE

C_T $\dfrac{T}{\rho \pi R^2 (\Omega R)^2}$, thrust coefficient

D Drag of the aircraft

$\vec{D}$ Vortex wake distortion as computed by the latest iteration, nondimensionalized by R

$\vec{D}'$ Vortex wake distortion as computed by the previous iteration, nondimensionalized by R

$\vec{D}''$ Combination of $\vec{D}$ and $\vec{D}'$ used to find $\vec{D2}$ and $\vec{D3}$

$\vec{D2}$ Vortex wake distortion of point P_ℓ, nondimensionalized by R

$\vec{D3}$ Vortex wake distortion of point P_η, nondimensionalized by R

$DI2, DJ2, DK2$ $\vec{i}, \vec{j}, \vec{k}$ components of $\vec{D2}$

$DI3, DJ3, DK3$ $\vec{i}, \vec{j}, \vec{k}$ components of $\vec{D3}$

$\vec{\Delta D}$ Nondimensional vortex wake distortion accumulated in time interval $\Delta\phi/\Omega$

M Number of turns (2π in azimuth) of the wake below point P_η considered in the integration of the Biot-Savart relation

P_η Point locating the element of vorticity whose wake distortion is being compu֡ ￼

P_ℓ Point locating the upper (larger azimuth)end of the voᵣtex segment whose induced velocity at point P_η is being computed

$\vec{Q}$ Induced velocity at point P_η due to a trailing vortex trailed from a given spanwise station on a given blade, nondimensionalized by ($\Gamma/4\pi R$)

R	Rotor radius
T	Rotor thrust
TPP	Tip path plane
V	Aircraft flight speed
W	Aircraft gross weight
a	$\frac{\partial C_L}{\partial \alpha}$, lift curve slope
a_o	Rotor blade coning angle, Fig. A1
$\vec{a}, \vec{b}$	Vectors from point P_η to the ends of the typical vortex segment, Fig. A2
b	Rotor blade semichord
$\vec{c}$	$\vec{a} - \vec{b}$, Fig. A2
$\vec{c}_1, \vec{c}_2$	$\vec{c}(\psi + \zeta + \Delta\phi)$, $\vec{c}(\psi + \zeta)$, Fig. A4
h	Perpendicular dropped from point P_η to the typical vortex segment
i	TPP incidence relative to free stream
$\vec{i}, \vec{j}, \vec{k}$	Unit vectors along x, y, z axes, Fig. A1
ℓ	Spanwise location of point P_ℓ at time t_ℓ, nondimensionalized by R
ℓ_I	Spanwise station from which the inboard vortex is trailed (normally 0.5), nondimensionalized by R
m	Number of turns (2π in azimuth) for which the wake distortion is calculated
n	An index
n_1	Number of $\Delta\phi$ intervals through which the blade is allowed to advance before $\vec{D}''$ is up-dated

$\vec{q}$ Induced velocity due to a single vortex segment, nondimensionalized by $(\Gamma/4\pi R)$

t_d Time at which the wake distortion at point P_η is calculated

t_ℓ Time at which the element of vorticity located at point P_ℓ was trailed

t_η Time at which the element of vorticity located at point P_η was trailed

x, y, z Coordinates of point P_ℓ relative to point P_η, Fig. A3

x_1, y_1, z_1 Coordinates of the end of the typical vortex segment which is not point P_ℓ, relative to point P_η, Fig. A3

Γ Circulation of a vortex segment

Ω Rotor angular velocity

$\alpha(\eta,\psi)$ Angle of attack

α,β Angles between $\vec{a}$ and $\vec{c}$ and between $\vec{b}$ and $\vec{c}$, Fig. A2

γ Circulation of a vortex segment, nondimensionalized by $2\pi b\Omega R$

ζ Angle between the η blade and the ℓ blade

η Spanwise location of point P_η at time t_η, nondimensionalized by R

η_R Root cutout of the rotor blade, nondimensionalized by R

λ Uniform, mean inflow from momentum theory, nondimensionalized by ΩR

μ Aircraft flight speed, nondimensionalized by ΩR

ρ_c	Vortex core radius, nondimensionalized by R
σ	Rotor solidity $\left(\dfrac{\text{blade area}}{\text{disk area}}\right)$
ϕ	Azimuth angle of the ℓ blade at time t_ℓ
ϕ'	Azimuth angle of the ℓ blade at time t_d
ϕ''	Azimuth angle of the ℓ blade, a dummy variable for integration
$\Delta\phi$	Azimuth angle subtended by a vortex segment $(\Delta\phi = \Delta\phi' = \Delta\phi'' = \Delta\psi)$
ψ	Azimuth angle of the η blade at time t_n

Subscripts

o	Time average value (zero'th harmonic)
BV	Bound vorticity
s	Shed wake
t	Trailing wake

I. INTRODUCTION

As rotary winged aircraft find wider applications greatly improved performance is being required of them, e.g., greater speed, better aerodynamic efficiency, and lower vibration levels. To meet these requirements, a better understanding of rotor aerodynamics is needed.

A recent major improvement has been the replacement of the classical uniform inflow assumption with the uniform inflow due to the tilt of the tip path plane (TPP) relative to the free stream plus the nonuniform induced inflow due to the vortex wake of the rotor. This induced inflow due to the vortex wake has been calculated, with the aid of high speed digital computers, by numerically integrating the Biot-Savart relation for the velocity induced by a vortex element over some assumed vortex wake geometry (e.g., see Refs. 1 through 4). The most common vortex wake geometry assumption has been a "rigid wake". This assumes that the vortex wake has the spiral shape traced out by a point on one of the rotor blades parallel to the tip path plane (TPP) and drifts perpendicularly to the TPP with the classical uniform inflow velocity. Reference 1 also tried a more refined approach which left the rigid wake assumption unchanged parallel to the TPP, but calculated the nonuniform induced inflow at the TPP using a rigid wake assumption and used this, or some of its harmonics, plus the uniform inflow component of the free stream to determine the drift velocity of the vortex wake perpendicular to the TPP.

The approach taken here is to assume a rigid wake and calculate the time history of induced velocity at various points in the wake. This is integrated to obtain an improved estimate of the wake geometry. This, in turn, is used to calculate a new time history of induced velocity, etc., and the iteration continues until convergence is achieved. Various refinements to improve convergence are required, but this iterative approach

1

still requires a good deal less computation than allowing the wake to distort continuously as the calculation of induced velocities proceeds, as in Ref. 9.

This report starts with a discussion of the choice of a model for the vortex wake. The development of the computational procedure used is outlined and some alternate techniques, now discarded, are discussed. Some preliminary results are presented and some recommendations are made for future development. The appendix presents a detailed outline of the computational procedure.

II. VORTEX WAKE MODEL

A detailed model for use in calculating rotor airloads would represent the rotor blades by lifting surfaces and the rotor wake by vortex sheets. The calculation of the wake geometry would involve the computation of the distortion and roll-up of these vortex sheets due to their own induced velocities and those of the lifting surfaces. As the vortex sheets rolled up into line vortices viscous effects would become important in the vortex core.

Unfortunately, the above model is far too ambitious for practical computations at present and a simplified model must be constructed. The rotor blades can be represented by lifting lines (bound vortices) instead of lifting surfaces. The vortex wake can be represented by a set of trailing and shed line vortices instead of vortex sheets. The trailing vortex lines are trailed aft along streamlines relative to the rotor blade while the shed vortex lines are shed parallel to the instantaneous position of the rotor blade.

For maximum thrust, the angle of attack and hence the bound circulation should be as nearly constant, radially, as possible over the outer portion of the blades, where most of the lift is generated. An idealized model of the radial bound circulation distribution on a rotor might have constant bound circulation from the 50 percent radius to the tip and zero circulation inboard. This would result in a pair of line vortices being trailed, one from the tip and one from the 50 percent radius.

A relatively sharp cutoff of the bound circulation at the tip of the rotor blade is normally obtained in actual rotor operation, and a concentrated tip vortex is observed (Ref. 5). The intersection, or near intersection, of this concentrated tip vortex with a rotor blade is thought to be a major cause of the high harmonic, almost impulsive, airloads observed in flight (Ref. 6). The location of this tip vortex is, therefore, likely to have a

3

considerable effect on the high harmonic airloads.

The inboard bound circulation, however, normally tapers off gradually in actual rotor operation, thus generating a broad vortex sheet. It is questionable whether this inboard vortex sheet ever rolls up tightly to become as concentrated as the tip vortex. In any case, it does not seem to roll up near enough to the rotor to induce large, high harmonic airloads similar to those induced by the tip vortex. Since the determination of the distortion and roll-up of the inboard vortex sheet requires too much computation for practical applications, and since the geometry of this inboard vortex sheet does not affect the airloads nearly as much as that of the tip vortex, the inboard vortex sheet is represented by a set of undistorted, rigid wake vortex lines.

Experience with rotor airload calculations has shown that for the far wake (the part of the wake more than 45 deg to 90 deg behind the rotor in azimuth), a two trailing vortex model (a tip vortex plus one inboard vortex) gives essentially the same results as a many trailing vortex model since the circulation is substantially constant along the blade. For the near wake (the first 45 deg to 90 deg in azimuth behind the rotor of the wake) a many trailing vortex model is often necessary in airload calculations when a rapid change in circulation exists. However, for a wake geometry calculation induced velocities are calculated on the tip vortex, not on the blade. Thus for computing the distortion of the tip vortex, a single, rigid wake inboard trailing vortex, typically trailed from the 50 percent spanwise station, represents the inboard trailing vortex sheet about as well as several rigid wake line vortices trailed from various inboard stations with a combined circulation equal to that of the tip vortex.

To compute the geometry of the tip vortex, the velocities induced on the tip vortex by itself, and by the inboard vortex,

4

must be calculated at various times. This computation involves
the integration of the Biot-Savart relation over the tip vortex
and the inboard vortex. Since this integral cannot be solved
analytically even for the relatively simple rigid wake case,
either the geometry of the tip vortex must be approximated by
some analytically integrable geometry or numerical integration
must be used. As shown in Ref. 7, the best method for integrating
the Biot-Savart relation in nonrigid wake cases is to break the
trailing vortex lines up into a set of short straight vortex line
segments each subtending an equal $\Delta\phi$ (typically $\Delta\phi = 15$ deg),
where ϕ is the azimuth angle. The shed vorticity can then be
represented by straight vortex line segments connecting the
corners where two trailing vortex line segments meet, both on
the tip vortex and the inboard vortex at the same azimuth angle
(ϕ). Figure 1 shows two turns (4π) of the spiral rigid wake of
one blade projected into the tip path plane (TPP), where $\ell = 1$
is the tip vortex and $\ell = 0.5$ is the inboard vortex trailed from
the 50 percent radius station.

The circulation of the various elements of vorticity in the
model must be defined for the computation of induced velocities.
The strength of the bound vortex as a function of azimuth angle
(time) is determined by a rotor airloads calculation using either
a distorted wake from a previous iteration of the wake geometry
computation or a rigid wake. The trailing wake vortex line seg-
ment between azimuth angles $\phi - \Delta\phi$ and ϕ is taken to have a con-
stant circulation equal to the circulation of the bound vortex at
azimuth angle ϕ. The shed wake vortex line segment at azimuth
angle ϕ is taken to have a constant circulation equal to the dif-
ference between the circulation of the trailing wake vortex line
segments between azimuth angles $\phi - \Delta\phi$ and ϕ and between azimuth
angles ϕ and $\phi + \Delta\phi$.

At low advance ratios (μ = flight speed/rotor tip speed)

5

when the effect of the self-induced velocities on the wake geome-
try is greatest, the bound circulation has a large steady state
value compared to its higher harmonics. A first approximation
for wake geometry calculations (as well as airload calculations,
see Ref. 2) is to assume a constant value of the bound circulation
based on the mean thrust of the rotor. This results in a trailing
wake where all of the vortex line segments have equal circulation
and eliminates the shed wake.

This vortex line representation is inadequate when it is
necessary to calculate the induced velocity at a point very close
to or on the tip vortex. For this case the effects of a finite
vortex core, where viscosity becomes important and the Biot-
Savart relation no longer applies directly, must be included. A
useful first approximation to the induced velocity inside a vor-
tex core is to assume solid body rotation of the vortex core with
an induced velocity at the outer edge of the vortex core equal to
the result given by the Biot-Savart relation at that point (see
Ref. 8). Thus for most cases it is only necessary to check
whether or not the point at which the induced velocity must be
calculated is inside the vortex core and apply either the Biot-
Savart relation or the solid body rotation model.

For the case of calculating the velocity induced at a point
(P) on the tip vortex by the two immediately adjacent vortex seg-
ments, the use of straight line vortex segments is inadequate,
since it would give zero induced velocity at point P due to these
two vortex segments. These two vortex segments adjacent to point
P are therefore replaced by a circular arc vortex segment passing
through the three points determined by the ends of the vortex
segments (see Fig. A4). The velocity induced at point P by the
circular arc vortex segment is given by Ref. 9 as a function of
the vortex core size, the radius of curvature, the circulation,
and the vortex segment size ($\Delta\phi$).

Various sources estimate the vortex core diameter at from 0.1 chord to 1.0 chord. Work is under way at MIT to refine the estimate of the vortex-core diameter, and to define the roll-up process in more detail. For the case of a rotor in forward flight, considered here, the results turn out to be very insensitive to vortex core size. For other cases, such as a highly loaded hovering propeller, the details of the rolling up of the tip vortex just after it is trailed are likely to be much more important.

Since the induced velocity calculated by the Biot-Savart relation falls off as 1/(distance) vortex elements far away from either the rotor or the portion of the wake being distorted contribute very little to the induced velocity. For airload calculations only the first two or three turns (2π in azimuth angle = 1 turn) of the wake are significant so that the wake geometry need only be calculated for this part of the wake. For wake distortion calculations only two or three turns of the wake below the wake element whose distortion is being calculated plus any wake above (nearer the rotor) the wake element need to be considered.

Consider the vortex element at the lower end(farthest away from the rotor) of the section of wake whose wake geometry is being calculated (two or three turns below the rotor). To calculate the distortion of this vortex element, two or three turns of the wake below this vortex element must be considered. For this additional section of the wake, an extrapolated version of the wake geometry must be used since its wake geometry cannot be calculated directly. The extrapolation procedure used here assumes that the wake has the same distortion parallel to the tip path plane as it had at the lower limit of the calculated wake geometry and drifts downward perpendicular to the tip path plane with the fully developed, uniform rotor inflow velocity from momentum theory.

7

III. DEVELOPMENT OF THE COMPUTATIONAL PROCEDURE

Having arrived at a model for the vortex wake of the rotor,
the calculation of the wake distortion due to self-induced ve-
locities can be considered. A straightforward way to do this is
to start with M (say M = 2 or 3) turns (2πM in azimuth) of rigid
wake and compute the velocity induced by this wake on the element
of the tip vortex which is just being trailed from the blade tip.
Advance the blade $\Delta\phi$ in azimuth, generating a new vortex line
segment, and compute the induced velocity at both the point where
it was calculated previously, which is now $\Delta\phi$ behind the blade,
and at the tip vortex element which is just being trailed from
the new blade position. Note that the calculation of the induced
velocity at the point $\Delta\phi$ behind the blade only requires the ad-
dition of the velocity induced by the newly generated vortex seg-
ment to that previously calculated for the rest of the wake. The
average of the two induced velocities calculated at the point $\Delta\phi$
behind the blade can be multiplied by the time interval $\Delta\phi/\Omega$ (where
Ω is the rotor angular velocity) to obtain the wake distortion at
this point during this time interval.

The blade is again advanced by $\Delta\phi$ and the induced velocity
is calculated at three points: at the blade tip, $\Delta\phi$ behind the
blade, and $2\Delta\phi$ behind the blade. Since the point $2\Delta\phi$ behind the
blade has moved relative to the rest of the wake, the induced
velocity at this point must be calculated by integrating over the
entire M turns of wake again. The distortion of the two points
$\Delta\phi$ and $2\Delta\phi$ behind the rotor is calculated as before.

This process of advancing the blade $\Delta\phi$ and calculating the
induced velocity and hence the wake distortion at an ever increas-
ing number of points continues until the distortion is being cal-
culated over m $\leq$ M turns (2πm in azimuth) of the wake. Then as
a new vortex segment, and hence point at which wake distortion is
calculated, is added at the beginning of the wake, the calculation

8

of the distortion of the point $2\pi m$ behind the rotor is stopped and the extrapolation procedure is applied as needed. This is because the wake geometry is only needed for the first m (typically m = 2) turns ($2\pi m$) of the wake, as discussed above. The blade continues to be advanced by $\Delta\phi$ and the wake distortion of the first m turns of the wake calculated until a stable wake geometry is arrived at.

While the process described above is easily programmed to be run on a digital computer, it requires a great deal of computation. For this reason, the above approach has not been tried at MIT. Instead, the initial approach assumed that the wake distortion from a rigid wake was small and an iterative procedure was chosen. This starts out just like the procedure outlined above but when the wake distortion is computed, it is merely stored and does not affect later induced velocity calculations. For the entire first iteration, a rigid wake is used for induced velocity calculations. When the blade has advanced through $2\pi m$ in azimuth (ϕ), the first iteration ends. The wake distortion is calculated from the time history of induced velocity obtained from the first iteration and is used to calculate a wake geometry which is then used for all induced velocity calculations in the second iteration. This process continues until convergence is achieved.

This iterative procedure saves a great deal of computation over the "run until stable" method since the points at which induced velocity is calculated do not move relative to the rest of the wake. Thus, the integration of the Biot-Savart relation over the entire wake does not have to be done repeatedly for the same point. Recall that "the entire wake" means, for all practical purposes, only M turns ($2\pi M$) of the wake below the point at which induced velocity is calculated and all of the wake above that point, as discussed previously.

In order to obtain converged solutions with this technique,

9

some refinements are needed. This is because of the [1/(distance)] variation of the Biot-Savart relation for induced velocities. When an element of the tip vortex finds itself in a region of high induced velocity, it is swept along rapidly with the induced velocity and is likely to find itself soon in a region with a considerably different induced velocity. In a method which only allows the wake to move relative to itself at the end of each iteration an element of vorticity which happens to be in a region of high induced velocity initially will remain there for the whole iteration and thus accumulate a large (and unrealistic) distortion.

An obvious way to improve this situation is to update the wake geometry being used to calculate induced velocities with the current calculated wake geometry every few (n_1) $\Delta\phi$. Thus every time the blade advances through $n_1\Delta\phi$ in azimuth the Biot-Savart relation must be integrated over the entire wake again, since the points at which induced velocities are calculated have moved relative to the rest of the wake. The key questions in this method are now how large can n_1 be and how many iterations are required for convergence (see the Results section of this report). This iterative method is our current approach for calculating wake geometry. Appendix A outlines the computational procedure in considerable detail.

IV. RESULTS

Some preliminary results, run to evaluate the relative importance of various parameters and approximations, are presented here. These preliminary results were all run for the same standard case (μ = 0.1125, λ = 0.04) to allow them to be compared with some experimental wake geometry results obtained by emitting smoke from the tip of one blade of a two-bladed rotor running in a wind tunnel. The wake geometry results are presented in the figures. Airloads have been computed using some of these theoretical wake geometry results but they are not presented here due to a lack of experimental airload data for comparison.

The experimental (test) data presented here is from some preliminary work to be reported in Ref. 11. This work is being continued under Army Research Office sponsorship (contract DA-31-124-ARO-D-470). The test data was obtained by ejecting hot oil smoke downstream from one blade tip of a two-bladed, articulated rotor operating in the return section (10 ft x 12 ft) of a closed circuit wind tunnel. Simultaneous photographs from below and from one side were taken and the coordinates of various points on the tip vortex were computed from this data with the aid of a high speed digital computer. These coordinates have been plotted and are the curves labeled "test" on the figures. Due to experimental difficulties, no data points were obtained in the dashed portion of the wake and this has been sketched in. Although the theoretical wake geometries are computed for a full 4π of the wake only 3π to 3.5π of test data have been obtained. The measured characteristics and operating conditions of the rotor for the standard case are: R = 2.425 ft., b = 0.125 ft., σ = 0.0657, Ω = 200 rpm, Locke Number = $2\rho\pi bR^4/I$ = 2.2, V = 353 fpm, θ(pitch angle) = 7.1 deg, i = $-$ 12.5 deg, α(shaft angle) = 15.1 deg. The calculated rotor operating conditions for the standard case are: μ = 0.1125, C_T = 0.0036, λ = 0.040, $-\mu$ tan i = 0.025, γ_o = 0.0465.

11

Due at least partly to wind-tunnel turbulence, the experimental wake geometry has not been found to be completely repeatable. Figure 2 shows a top view (in the TPP) and a side view of the tip vortex of one blade of a two-bladed rotor for two different experimental wake geometries and rigid wake, all for the standard case. It can be seen that the two typical test results have the same general character but differ in detail. One of these test results is used for comparison with the theoretical wake geometry in Figs. 3 through 8. When comparing theory and experiment it will be necessary to look for the same kind of agreement in general character rather than complete, detailed agreement because of this uncertainty in the experimental results.

The theoretical calculations whose results are presented here (Figs. 3 through 8) have all used $m = 2$, $M = 3$, and $\Delta\phi = 15$ degs, chosen from experience with previous wake geometry programs. These results are intended to illustrate the effects of various approximations and parameters on the calculated wake geometry. Figures 3 through 8 all compare a theoretical result with an experimental (test) result and with a $\lambda = 0.04$ rigid wake.

It should be noted that while the figures all show the wake geometry when the blade is at $\psi = 345$ degs for comparison with experiment, the geometry changes as the blade takes different azimuth positions. Thus a complete description of the wake geometry would require a separate figure for every blade azimuth position $0 \leq \psi \leq 2\pi$. The computer calculation necessarily generates the information needed to construct such plots every $\Delta\psi$ (15 deg) but they are not presented here.

Figures 3, 4, and 5 show the effect of varying n_1 on the calculated wake geometry. They all represent essentially converged solutions, use a nondimensional vortex core radius $\rho_c = 0.05$, neglect bound vorticity, and assume a constant strength trailing wake ($\gamma_t = 1.0$), which implies no shed wake ($\gamma_s = 0.0$).

12

Figure 3 presents the results of the fourth iteration, $n_1 = 2$;
Fig. 4 presents the results of the fifth iteration, $n_1 = 6$, and
Fig. 5 presents the results of the fifth iteration $n_1 = 12$. Note
that the $n_1 = 2$ case required one less iteration for convergence.
Convergence is determined by comparing the plotted results of
successive iterations and hence is somewhat subjective. The total
running time on the MIT Computation Center's IBM 7094 to produce
the final, converged results was approximately:

n_1	2	6	12
Computer Time (min.)	56	25	14

Comparing Figs. 3, 4, and 5 it is seen that $n_1 = 2$, and $n_1 = 6$
give very similar results, especially in the side view, while
$n_1 = 12$ gives somewhat different results, notably in the side
view. In the $n_1 = 12$ case part of the wake is predicted to be
much closer to the TPP than it should be or than predicted by
$n_1 = 2$ and $n_1 = 6$. Thus $n_1 = 6$ is recommended to obtain acceptable
accuracy for most purposes while requiring less than 1/2 as much
computer running time as the $n_1 = 2$ case.

It might be argued that, since the tip vortex is by far
the most important part of the vortex wake, perhaps the rest of
the vortex wake can be neglected, at least for the purpose of
computing the geometry of the tip vortex. This has been tried and
Fig. 6 shows the result of the third iteration, $n_1 = 2$, $\rho_c = 0.05$,
$\gamma_t = 1.0$, $\gamma_s = 0.0$, with bound vorticity neglected, and with
$\ell = 1.0$ only instead of the usual $\ell = 1.0$ and 0.5. This result has
not converged and comparison with the second iteration (not pre-
sented here) seems to indicate that it is diverging at least over
the part of the tip vortex farthest from the blade in azimuth.
In any case the results are sufficiently different from the $\ell =$
1.0 and 0.5 case (Fig. 3) to indicate that the inboard ($\ell = 0.5$)
vortex cannot be neglected.

Figure 7 shows the results of the second iteration, $n_1 = 6$,

13

ρ_c = 0.05, including bound vorticity and with the γ_t and γ_s determined by a rigid wake airloads calculation. Note that convergence only required two iterations as compared to five for the γ_t = 1.0, γ_s = 0.0 case. This is believed to be due to the damping effect of the shed wake. The total running time to convergence on an IBM 7094 was approximately 13 minutes plus less than one minute to compute the γ_t and γ_s. Thus because of its much faster convergence, this case requires less computation to obtain a converged result than the γ_t = 1.0, γ_s = 0.0 case in spite of . the greater computation required for each interation. Comparison of this result (Fig. 7) with the γ_t = 1.0, γ_s = 0 case (Fig. 4) shows similar agreement with the test results.

Figure 8 presents the results of the same case as Fig. 7 but with ρ_c = 0.005 instead of ρ_c = 0.05 to check the effect of different tip vortex core radius estimates on the calculated wake geometry. Comparison of these figures shows negligible difference, which is fortunate since there is about an order of magnitude uncertainty in ρ_c.

14

V. CONCLUSIONS AND RECOMMENDATIONS

The work reported here is continuing and this is a pre-
liminary report. At present, a reasonable model of the vortex
wake has been developed, a method of computing the geometry of
the tip vortex has been developed, and the relative importance of
various parameters and approximations used by this method has
been evaluated for one test case including comparison with an ex-
perimentally determined tip vortex geometry. As a result of this
work some preliminary conclusions can be drawn and some sugges-
tions for further refinement of the vortex wake model and the
wake geometry computation procedure can be made.

1) Although the tip vortex is the dominant feature of the
   vortex wake, some representation of the inboard trailing
   vorticity must be included. This representation of the
   inboard trailing vorticity can be fairly crude (for
   example: a single vortex line trailing from the 50 per-
   cent span point) and if it is, then the use of an a priori
   specification of its geometry, such as the rigid wake ap-
   proximation is entirely adequate. A possible improve-
   ment over a single vortex trailing from the 50 percent
   span point, which has not been tried yet, would be a
   set of rectangular trailing vortex sheets trailed at
   constant (spanwise) strength between, for example, the
   30 percent span point and the 70 percent span point.
   The downstream dimension of the rectangles might be
   taken as $0.5R \, \Delta\phi$ or $0.7R \, \Delta\phi$. This would imply some
   overlapping and/or gaps between the vortex sheets
   but it should still be a better model than a single
   trailing vortex line without requiring as much extra
   computation as multiple trailing vortex lines.

2) The effects of a time varying trailing wake circula-
   tion and the corresponding shed wake should be included.

15

The current model which accumulates the shed wake in a
series of line vortices joining the corners of the
trailing wake model (see Fig. 1) is adequate but a
possible improvement,which has not been tried yet,
would be a set of rectangular shed vortex sheets
similar to the trailing vortex sheets mentioned above.

3) The calculated vortex wake geometry is very insensi-
tive to the estimated vortex core size and any vortex
core radius from 1.0 to 0.1 chord gives essentially
the same results.

4) For the updating interval used in the wake distortion
calculation, n_1 (see Page 10), a value of $n_1 = 6$ is a
good compromise between computation time and accuracy.

A great deal remains to be done. Although the current
computer program requires less than 15 min running time on an
IBM 7094 for a two-blade case, considerable improvement in this
respect is still required before extensive application of this
technique becomes practical. A promising way of improving the
current computational procedure, which is now being tried, is to
revise the method of determining when the wake distortion used
for computing induced velocities ($\overrightarrow{D''}$) is updated to the latest
calculated wake distortion ($\overrightarrow{D}$). This is currently done at fixed
times whenever the ℓ blade advances $n_1 \Delta \phi$ (see Pages 10 and 36).
It is proposed to keep track of the distortion accumulated at
each azimuth angle (ψ) since the last updating of $\overrightarrow{D''}$ for that ψ.
Whenever the magnitude of this accumulated distortion exceeds
some limit (D_L) then $\overrightarrow{D''}$ at that ψ only would be updated to the
latest $\overrightarrow{D}$. D_L is a parameter similar in function, but not in magni-
tude, to n_1 in the current program. The best value to use for
D_L will have to be determined by trial in a manner similar to the
determination of $n_1 = 6$ as a good compromise in the Results sec-
tion of this report. Just how much reduction in running time will

16

result from this new refinement ;mains to be seen but it is expected to be considerable.

An alternate way to reduce the computational effort required to obtain the wake geometry and, if feasible, the most useful approach for practical applications would be to develop a quasi-empirical way of obtaining an a priori specification of the wake geometry, in effect a better rigid wake approximation. This could be developed by building up experience as to what kind of wake geometries can be expected in various flight conditions, using both experimental data from flow visualization studies and theoretical results obtained by computations similar to those described in this report. Then using physical reasoning, plus perhaps some simple analytical approximations, the desired specification of the wake geometry wou] ' be developed.

Since the wake geometry is only important to the extent that it influences the airloads on the rotor (or fuselage) a study of the influence of the wake geometry on the airloads is necessary. This will determine just how good a quasi-empirical specification of the wake geometry must be and what portions of the wake geometry are the most important. An experimental program where the airloads on a rotor are measured by pressure transducers at the same time as the geometry of the tip vortex is determined by flow visualization would be very useful in support of this effort.

A question which has not been considered here but which is vital to a full understanding of rotor airloads and noise is that of short range blade-vortex interaction. Due to wake distortion, a rotor blade occasionally passes very near to or intersects the tip vortex. This results in large airload peaks and considerable amounts of very objectionable noise. It may also cause the breakdown of the tip vortex locally with a resultant effect on the airloads and the wake geometry. This problem is exceedingly

17

complex and will require the representation of the blade by a
lifting surface and probably the consideration of both viscosity
and Mach number effects. The ultimate aim of work on this prob-
lem should be a good enough understanding of the problem to allow
the formulation of simple quasi-empirical approximations for the
airloads and noise generated by these interactions and to indicate
what happens to the vortex after such an interaction.

18

REFERENCES

1. Miller, R.H. "Rotor Blade Harmonic Airloading." _AIAA Journal_ 2, 1254-1269 (July 1964).

2. Miller, R.H. "Unsteady Air Loads on Helicopter Rotor Blades." Fourth Cierva Memorial Lecture, _Journal of the Royal Aeronautical Society_ 68, 217-229 (April 1964).

3. Segel, L. "A Method for Predicting Nonperiodic Air Loads on a Rotary Wing." _Journal of Aircraft_ 3, 541-548 (Nov.-Dec. 1966).

4. Piziali, R.A., and DuWalt, F.A. _A Method for Computing Rotary Wing Air Load Distribution in Forward Flight._ Transportation Research Command Rept. Tr-62-44 (Nov. 1962).

5. Tararine, S. and Delest, M. _Experimental and Theoretical Study of Local Induced Velocities Over a Rotor Disk for Analytical Evaluation of the Primary Loads Acting on Helicopter Rotor Blades._ Giravios Dorand Rept. DE2012 (1960).

6. Scheiman, T. and Ludi, L.H. _Qualitative Evaluation of Effect of Helicopter Rotor Blade Tip Vortex on Blade Air Loads._ NASA TN D-1637 (May 1963).

7. Scully, M.P. _Approximate Solutions for Computing Helicopter Harmonic Air Loads._ Massachusettts Institute of Technology Aeroelastic and Structures Research Laboratory Technical Report 123-2 (Dec. 1965).

8. Prandtl, L. and Tietjens, O.G. _Fundamentals of Hydro- and Aeromechanics_, sec. 89, Dover, (1934).

9. Crimi, P. _Prediction of Rotor Wake Flows._ CAL/USAAVLABS Symposium Proceedings, Aerodynamic Problems Associated with V/STOL Aircraft, Vol. 1 (June 1966).

19

10. Glauert, M. <u>The Elements of Aerofoil and Airscrew Theory</u>. Cambridge University Press (1959).

11. Stoddard, F. and Thompson, T. <u>Flow Visualization Studies of Helicopter Tip Vortices</u>. Massachusetts Institute of Technology Aeroelastic and Structures Research Laboratory Technical Report 142-1 (September 1967).

SHED VORTEX SEGMENT AT AZIMUTH ANGLE ϕ

ℓ=1.0 TRAILING VORTEX SEGMENT AT AZIMUTH ANGLE ϕ

ℓ=0.5 TRAILING SEGMENT AT AZIMUTH ANGLE $\phi - \Delta \phi$

BOUND VORTEX

ROTOR BLADE

ROTOR HUB
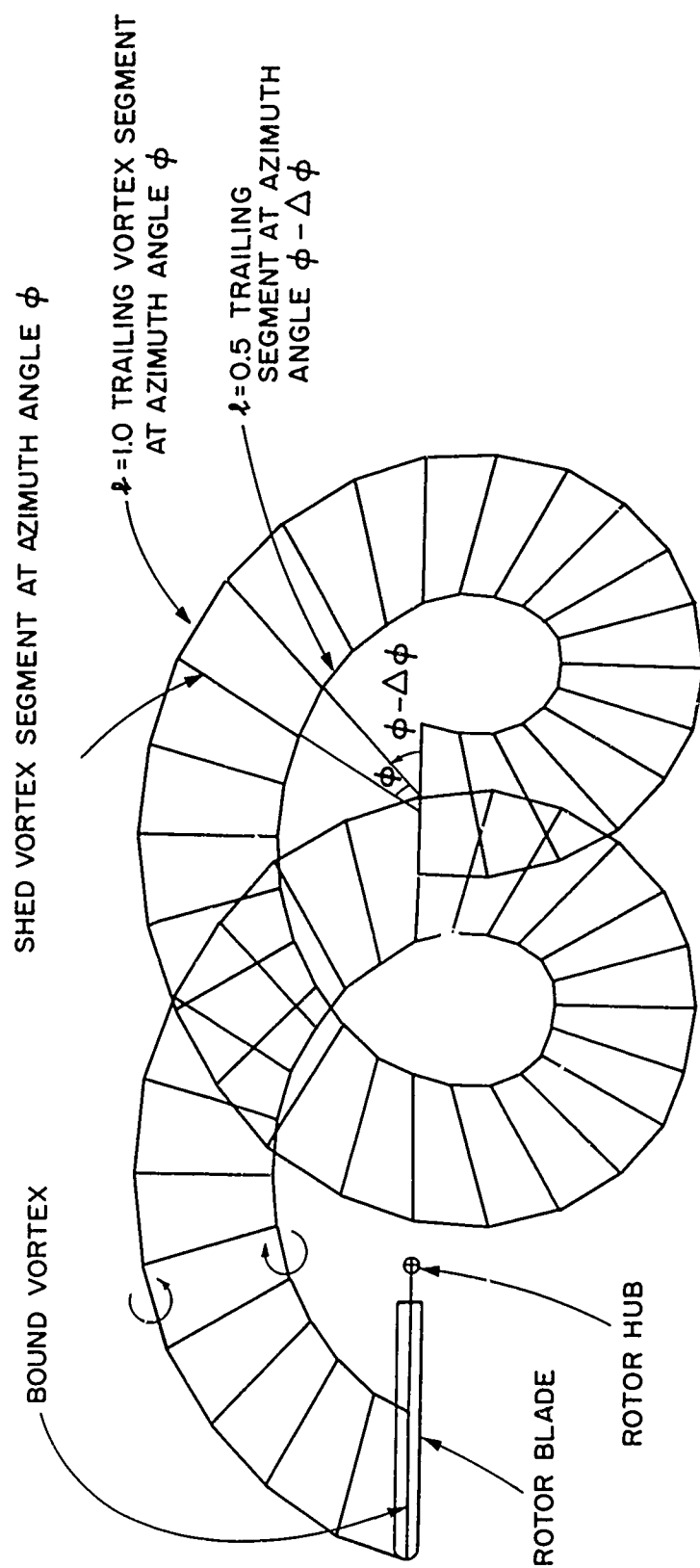
FIGURE 1: MODEL OF THE FIRST 4π OF THE WAKE OF ONE BLADE PROJECTED INTO THE TPP (RIGID WAKE)

ROTOR BLADE

VIEW IN TPP

ROTOR HUB   TPP

SIDE VIEW

——— TEST   ——— RIGID WAKE

FIGURE 2 :   COMPARISON OF TEST (FLOW VISUALIZATION) RESULTS

22

VIEW IN TPP

SIDE VIEW

FIGURE 3 COMPARISON OF THEORY AND TEST RESULTS –
$n_1 = 2$, 4th ITERATION, $\rho_c = 0.05$, $\gamma_t = 1.0$,
$\gamma_s = 0.0$, AND $\ell = 1.0, 0.5$

23

VIEW IN TPP

SIDE VIEW

FIGURE 4 COMPARISON OF THEORY AND TEST RESULTS –
$n_l = 6$, 5th ITERATION, $\rho_c = 0.05$, $\gamma_t = 1.0$, $\gamma_s = 0.0$,
AND $\ell = 1.0, 0.5$

VIEW IN TPP

SIDE VIEW
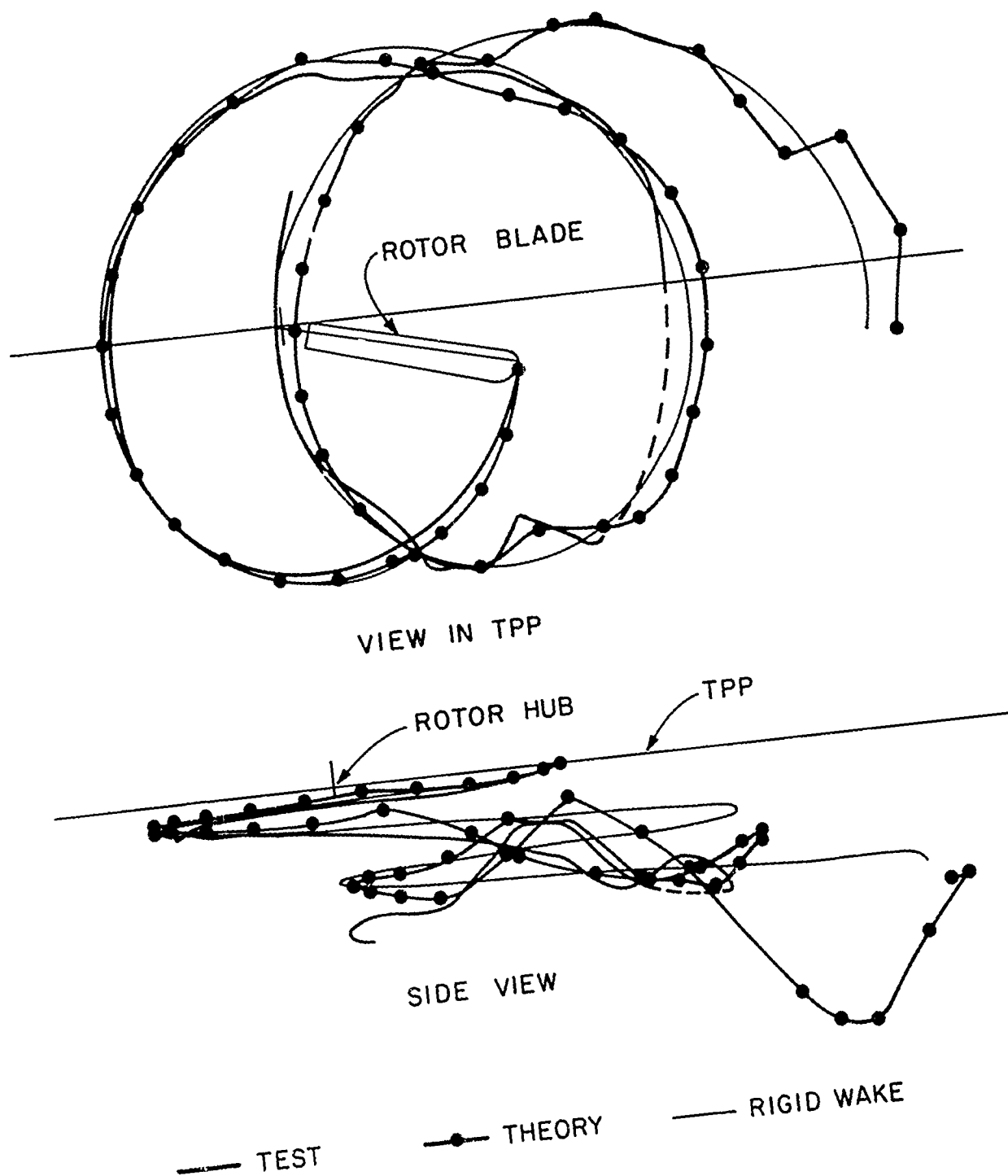
— TEST   •—• THEORY   —— RIGID WAKE

FIGURE 5   COMPARISON OF THEORY AND TEST RESULTS-
$n_1 = 12$, 5th ITERATION, $\rho_c = 0.05$, $\gamma_t = 1.0$, $\gamma_s = 0.0$,
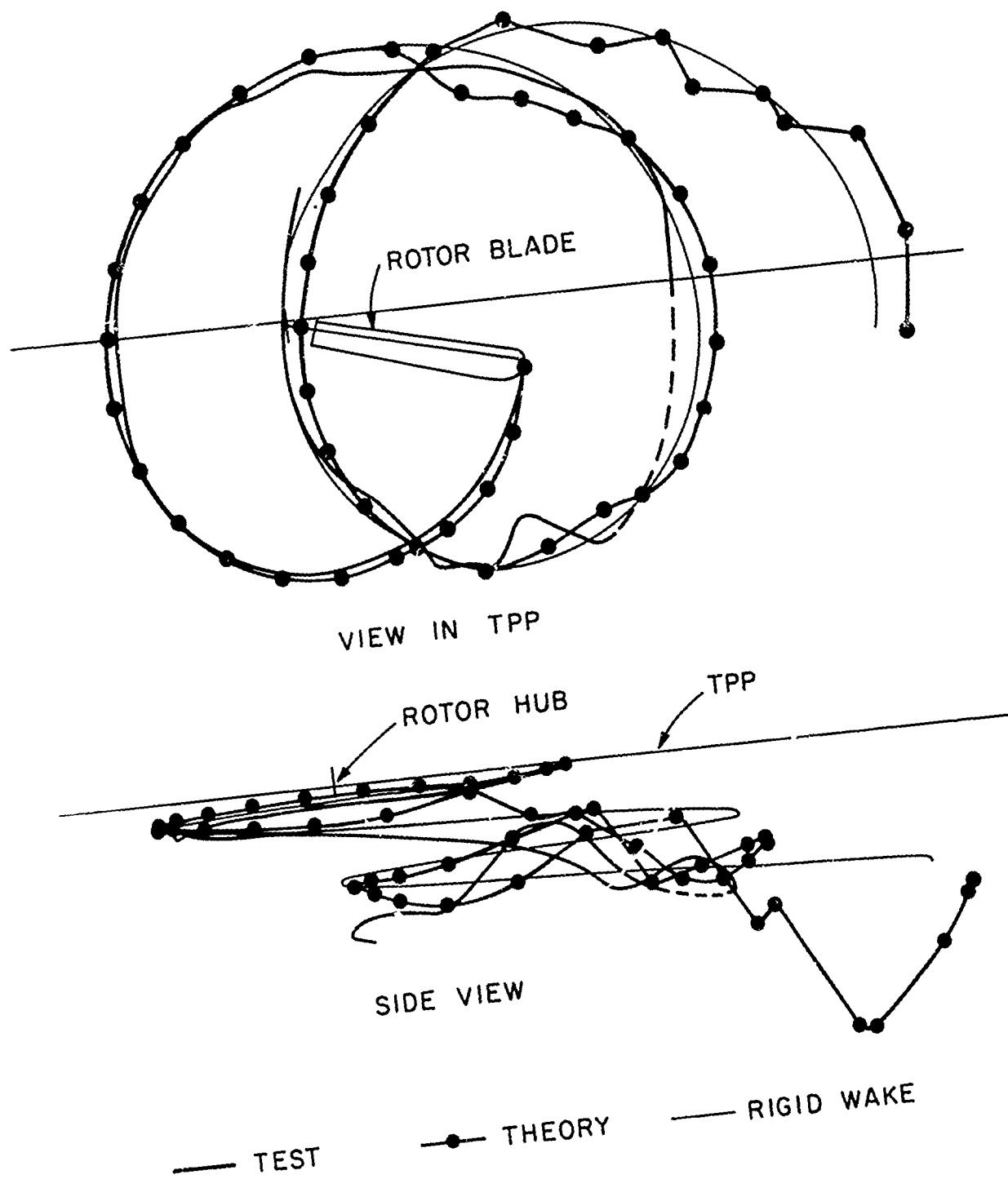AND $\ell = 1.0, 0.5$

ROTOR BLADE

VIEW IN TPP

ROTOR HUB   TPP

SIDE VIEW

—— TEST   —•— THEORY   —— RIGID WAKE

FIGURE 6   COMPARISON OF THEORY AND TEST RESULTS –
$n_1 = 2$, 3rd ITERATION, $\rho_c = 0.05$, $\gamma_t = 1.0$,
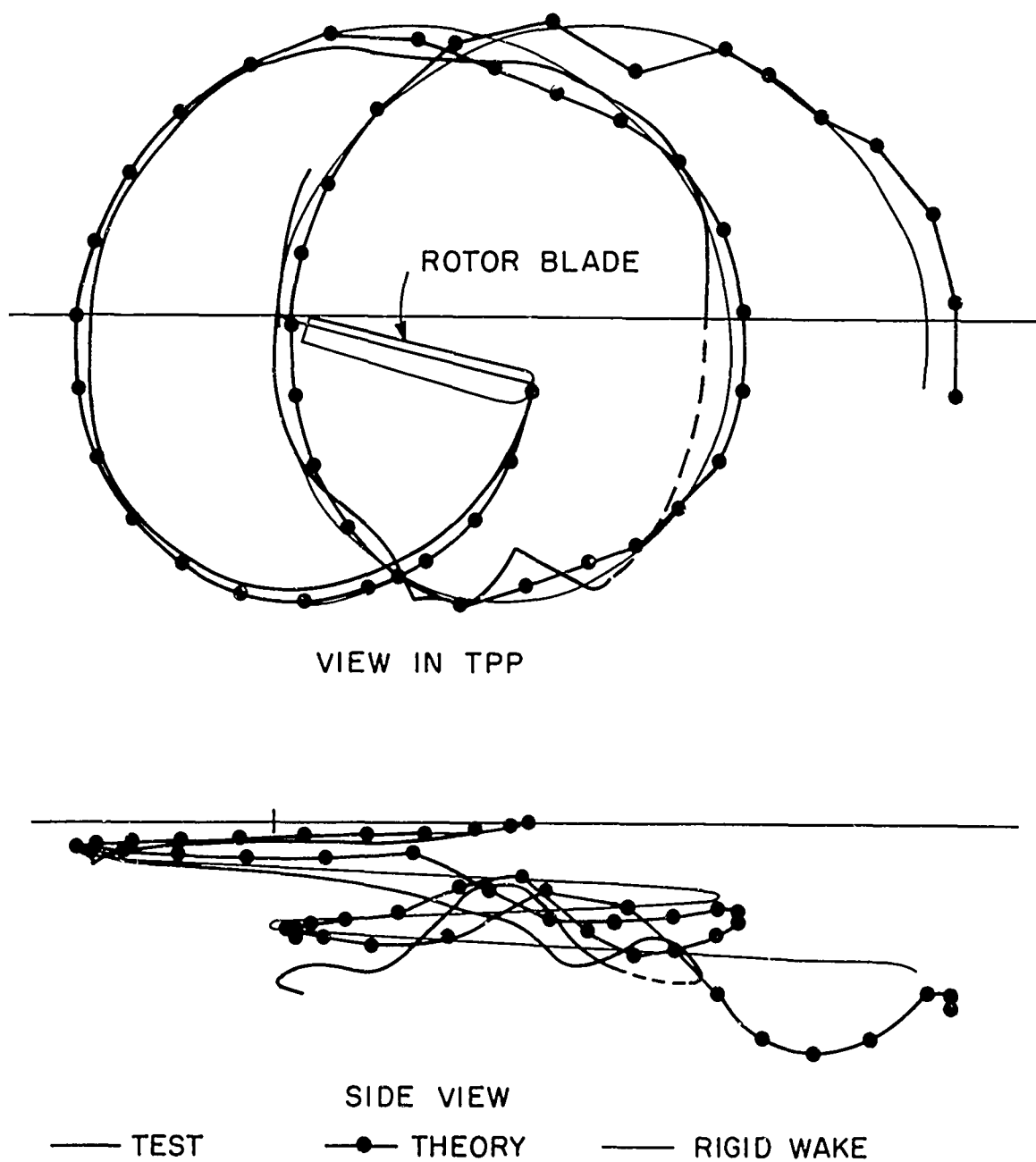$\gamma_s = 0.0$, AND $\ell = 1.0$

26

ROTOR BLADE

VIEW IN TPP

SIDE VIEW

—— TEST   —•— THEORY   —— RIGID WAKE

FIGURE 7 COMPARISON OF THEORY AND TEST RESULTS –
$n_1 = 6$, 2nd ITERATION, $\rho_c = 0.05$, γ_t AND γ_s FROM
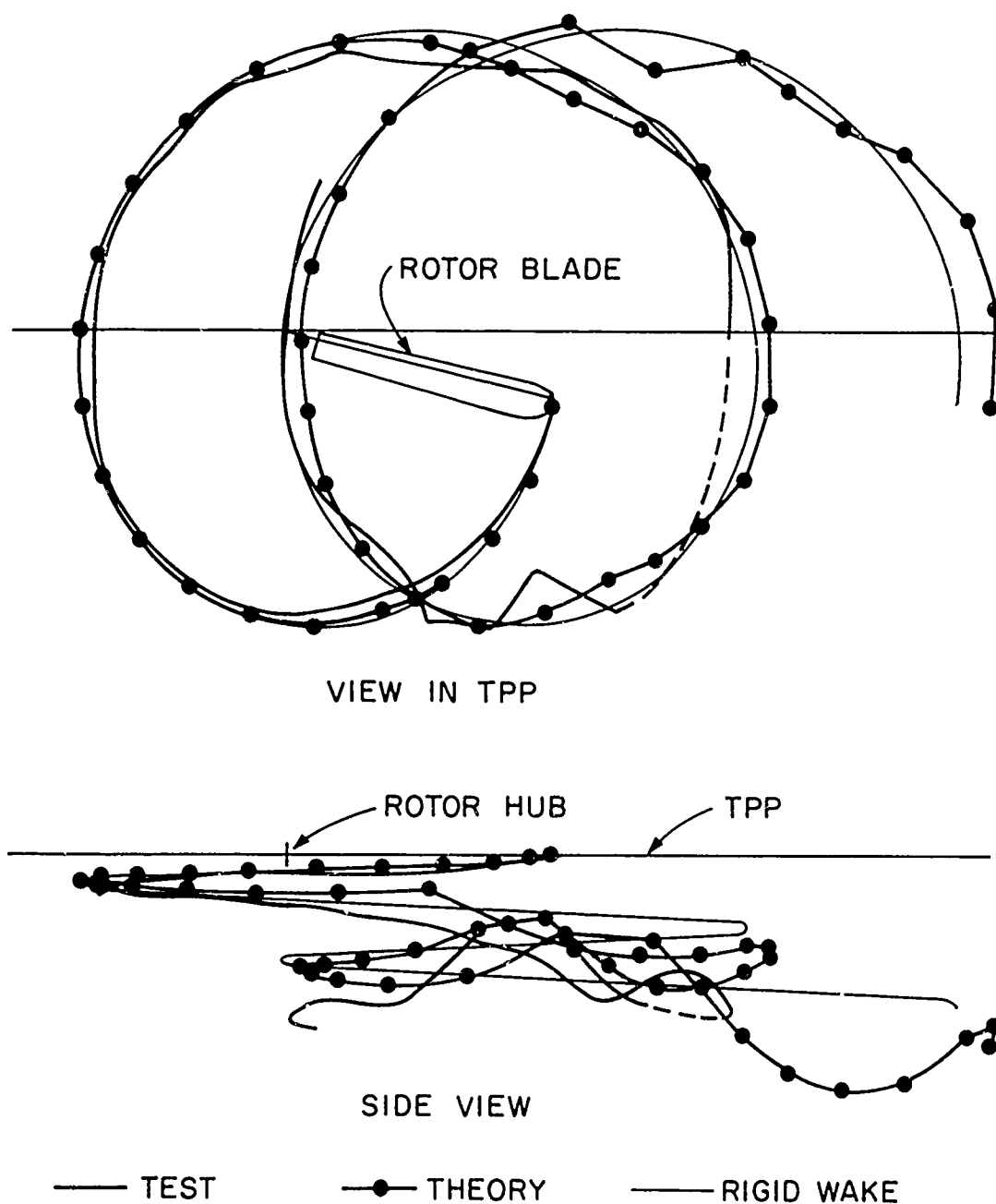RIGID WAKE AIRLOADS, AND $\ell = 1.0$, 0.5

27

FIGURE 8   COMPARISON OF THEORY AND TEST RESULTS –
$n_1 = 6, 2^{nd}$ ITERATION, $\rho_c = 0.005$, γ_t AND γ_s FROM
RIGID WAKE AIRLOADS , AND $\ell = 1.0$, 0.5

APPENDIX

THE COMPUTATIONAL PROCEDURE

The vortex wake geometry can be broken up into two parts: the basic geometry due to the motion, relative to the free stream, of those portions of the rotor blades from which the wake is trailed, and the wake distortion due to the velocity field induced by the wake and the bound vorticity. This division of the wake geometry is convenient since the basic geometry is easily calculated for a given advance ratio ($\mu = V/\Omega R$) and tip path plane incidence relative to the free stream (i), see Fig. A1, allowing effort to be concentrated on the calculation of the wake distortion.

For the computation of the nondimensional wake distortion ($\vec{D}$) of point P_n on the vortex wake, a coordinate system is chosen with its origin at the point where P_n would be if only the basic geometry was considered. A right-handed axis system is defined with the y axis and $\vec{j}$ parallel to and in the opposite direction from the line of rotor hub motion and parallel to the tip path plane (TPP). The x axis and $\vec{i}$ are perpendicular to the y axis and are parallel to the TPP. The z axis and $\vec{k}$ are perpendicular to the TPP and point downward (see Fig. A1). $\vec{i}$, $\vec{j}$, and $\vec{k}$ are unit vectors.

Let the time at which the wake distortion of point P_n is calculated be t_d. Let the time at which the element of vorticity at point P_n was trailed be t_n. Then at time t_n point P_n was located on a radial spanwise line from the center of the rotor hub (representing the quarter-chord line of the blade), at a distance nR ($n = 1.0$ for the tip vortex), from the hub on the blade with azimuth angle ψ(the n blade), where R is the rotor radius.

Consider a typical vortex segment, whose induced velocity at P_n must be calculated. Let the time at which the last element

29

of vorticity forming part of the vortex segment was trailed be
t_ℓ. If the location of this element of vorticity is labeled P_ℓ
then at time t_ℓ point P_ℓ was located on a radial spanwise line
from the center of the rotor hub (representing the quarter-chord
line of the blade), at a distance ℓR from the hub on the blade
with azimuth angle ϕ (the ℓ blade). Note that the first element
of this vortex segment was trailed at time $t_\ell - \Delta\phi/\Omega$ when the
ℓ blade was at azimuth angle $\phi - \Delta\phi$ (Ω = rotor angular velocity,
radians/sec).

Let the instantaneous angle between the η blade and the ℓ
blade be ζ. Then $t_\eta - t_\ell = (\psi + \zeta - \phi)/\Omega$, for example.

The distortion, at time t_d, of the element of the tip vor-
tex located at point P_η is a function of two variables. One is
the azimuth angle (ψ) of point P_η at the instant of trailing (t_η).
The other is the time since the element of vorticity was trailed
$t_d - t_\eta = (\phi' - \psi - \zeta)/\Omega$, where ϕ' is the azimuth angle of the ℓ
blade at time t_d. The range of ($\phi' - \psi - \zeta$) is determined by the
number of turns of the wake (m) whose distortion is calculated
$0 \leq (\phi' - \psi - \zeta) \leq 2\pi m$, while the range of ψ is $0 \leq \psi \leq 2\pi$.

The nondimensional total wake distortion ($\vec{D}$) is the sum of
the nondimensional distortions due to the trailing wake ($\vec{D}_t$),
the shed wake ($\vec{D}_s$), and the bound vorticity ($\vec{D}_{BV}$).

$$\vec{D} = \vec{D}_t + \vec{D}_s + \vec{D}_{BV}$$

The wake distortion due to the trailing wake is the distor-
tion which accumulates in time $\Delta\phi/\Omega$ due to the vortex trailed
from the ℓth spanwise station on the ζth blade summed over time,
both ℓ, and all ζ.

$$\vec{D}_t(\psi, \phi' - \psi - \zeta) = \sum_s \sum_\ell \sum_{\phi'' = \psi + \zeta + \Delta\phi}^{\phi'} \Delta\vec{D}_t(\ell, \zeta, \psi, \phi'')$$

30

The summation over ϕ'' (time) represents the integration of the induced velocity over time while the η blade moves from azimuth angle ψ at time t_η to azimuth angle $\phi' - \zeta$ at time t_d. This is the same as the ℓ blade moving from $\psi + \zeta$ to ϕ'.

Similarly, the wake distortion due to the shed wake is the distortion which accumulates during time $\Delta\phi/\Omega$ due to the shed wake trailed by the ζth blade summed over time and all ζ.

$$\vec{D}_s(\psi, \phi' - \psi - \zeta) = \sum_{\zeta} \sum_{\phi'' = \psi + \zeta + \Delta\phi}^{\phi'} \Delta\vec{D}_s(\zeta, \psi, \phi'')$$

The nondimensional wake distortion due to the bound vorticity is:

$$\vec{D}_{BV}(\psi, \phi' - \psi - \zeta) = \sum_{\zeta} \sum_{\phi'' = \psi + \zeta + \Delta\phi}^{\phi'} \Delta\vec{D}_{BV}(\zeta, \psi, \phi'')$$

Note that no sum over ℓ is needed for the shed wake or the bound vorticity since for the 2ℓ case considered here there is only one element of shed wake or bound vorticity at any azimuth (see Fig. 1). In all three cases above, the sum on ϕ'' starts at $\psi + \zeta + \Delta\phi$ because at $\phi'' = \psi + \zeta$ no time has elapsed since P_η was trailed and hence no distortion has occurred. Thus, when $\phi' = \psi + \zeta$, set $\vec{D}(\psi, \phi' - \psi - \zeta) = 0$ for all $\psi(0 \leq \psi \leq 2\pi)$.

Let the nondimensional induced velocity at point P_η at the instant when the ℓ blade has azimuth angle ϕ'' due to the vortex trailed from the ℓth spanwise station on the ζth blade be $\vec{Q}(\ell, \zeta, \psi, \phi'')$. Assuming that the average $\vec{Q}$ in a time interval $\Delta\phi/\Omega$ is the average of the $\vec{Q}$ at the beginning and end of that time interval:

31

$$\Delta \vec{D}_t(\ell, s, \psi, \phi'') = \frac{1}{2} \gamma_o \frac{b}{2R} \left[\vec{Q}(\ell, s, \psi, \phi'') + \vec{Q}(\ell, s, \psi, \phi'' - \Delta\phi) \right] \Delta\phi$$

where b is the blade semichord, $\gamma_o = \dfrac{\Gamma_o}{2\pi b \Omega R}$ and Γ_o is the time average bound circulation. The nondimensional induced velocity due to the individual vortex segments ($\vec{q}_t$) is summed to obtain $\vec{Q}$:

$$\vec{Q}(\ell, s, \psi, \phi'') = \sum_{\phi = \psi + s - 2\pi M + \Delta\phi}^{\phi''} \gamma_t(\ell, \phi)\, \vec{q}_t(\ell, s, \psi, \phi)$$

where $\gamma_t(\ell, \phi) = \Gamma_t(\ell, \phi)/\Gamma_o$ and Γ_t is the circulation of an individual trailing vortex segment.

Averaging is not used for the shed wake, therefore:

$$\Delta \vec{D}_s(s, \psi, \phi'') = \gamma_o \frac{b}{2R} \left[\sum_{\phi = \psi + s - 2\pi M}^{\phi'' - \Delta\phi} \gamma_s(\phi)\, \vec{q}_s(s, \psi, \phi) \right] \Delta\phi$$

where $\gamma_s(\phi) = \Gamma_s(\phi)/\Gamma_o$, Γ_s is the circulation and $\vec{q}_s$ is the nondimensional induced velocity of an individual shed vortex segment.

For the bound vorticity no sum over ϕ is needed.

$$\Delta \vec{D}_{BV}(s, \psi, \phi'') = -\gamma_o \frac{b}{2R} \gamma_t(1.0, \phi'')\, \vec{q}_s(s, \psi, \phi'') \Delta\phi$$

From Ref. 10, the induced velocity at point P_η due a vortex segment of circulation Γ is perpendicular to the plane formed by the vortex segment and point P_η and has the magnitude

32

$$\left(\frac{\Gamma}{4\pi R}\right)\left(\frac{\cos\alpha + \cos\beta}{h/R}\right)$$ (see Fig. A2). The induced velocity nondimensionalized by $(\Gamma/4\pi R)$ is then:

$$\vec{q} = \left(\frac{\cos\alpha + \cos\beta}{h/R}\right)\vec{n} = \left[\frac{\dfrac{(-\vec{a})\cdot(-\vec{c})}{|\vec{a}|} + \dfrac{(-\vec{b})\cdot\vec{c}}{|\vec{b}|}}{|(-\vec{c})\times(-\vec{a})|}\right]\frac{\vec{a}\times\vec{b}}{|\vec{a}\times\vec{b}|}$$

see Fig. A2.

Let $\vec{a}_t$, $\vec{b}_t$, and $\vec{c}_t$ be used to define $\vec{q}_t$ and $\vec{a}_s$, $\vec{b}_s$, and $\vec{c}_s$ to define $\vec{q}_s$. For the trailing wake:

$$X = X(l,\phi), \quad y = y(l,\phi),$$
$$z = z(l,\phi), \quad X_1 = X(l,\phi-\Delta\phi), \quad y_1 = y(l,\phi-\Delta\phi),$$

and $z_1 = z(l,\phi-\Delta\phi)$. Then from Fig. A2:

$$\vec{a}_t = X(l,\phi)\vec{\imath} + y(l,\phi)\vec{\jmath} + z(l,\phi)\vec{k},$$
$$\vec{b}_t = X(l,\phi-\Delta\phi)\vec{\imath} + y(l,\phi-\Delta\phi)\vec{\jmath} + z(l,\phi-\Delta\phi)\vec{k},$$
$$\vec{c}_t = \vec{a}_t - \vec{b}_t.$$

For the shed wake: $X = x(1.0,\phi)$,

$$y = y(1.0,\phi), \quad z = z(1.0,\phi), \quad X_1 = X(0.5,\phi), \quad y_1 = y(0.5,\phi)$$
$$z_1 = z(0.5,\phi).$$

From Fig. A2:
$$\vec{a}_s = X(1.0,\phi)\vec{\imath} + y(1.0,\phi)\vec{\jmath} + z(1.0,\phi)\vec{k},$$
$$\vec{b}_s = X(0.5,\phi)\vec{\imath} + y(0.5,\phi)\vec{\jmath} + z(0.5,\phi)\vec{k}, \quad \vec{c}_s = \vec{a}_s - \vec{b}_s$$

Let the nondimensional distortion of point P_l be
$$\vec{D2} = DI2\,\vec{\imath} + DJ2\,\vec{\jmath} + DK2\,\vec{k}$$ and that of point P_n be
$$\vec{D3} = DI3\,\vec{\imath} + DJ3\,\vec{\jmath} + DK3\,\vec{k}.$$

From Fig. A3:
$$X(l,\phi) = l\sin\phi - \sin\psi + DI2 - DI3,$$
$$y(l,\phi) = l\cos\phi - \cos\psi + \mu(\psi+S-\phi) + DJ2 - DJ3.$$

Recalling that the tilt of the tip path plane relative to the free stream (Fig. A1) causes a displacement of the wake in the z direction of $-\mu\tan i\ (\psi + 5 - \phi)$ similar to the $\mu(\psi + 5 - \phi)$ term in the $y(\ell, \phi)$ equation (recall: $t_\eta - t_\ell = (\psi + 5 - \phi)/\Omega$):

$$z(\ell, \phi) = -\mu\tan i\ (\psi + 5 - \phi) + a_o(\ell - 1.0) + DK2 - DK3,$$

where a_o is the coning angle (see Fig. A1).

When $\dfrac{h}{R} = \dfrac{|(-\vec{c}) \times (-\vec{a})|}{|\vec{c}|} < \rho_c$ point P_η is inside the vortex core, where $\rho_c R$ is the radius of the core of the tip vortex and a modified definition of $\vec{q}$ is needed (see Page 6). First the induced velcity ($\vec{q}_{\rho_c}$) at $h/R = \rho_c$, the edge of the vortex core is determined.

$$\vec{q}_{\rho_c} = \left[\frac{\dfrac{c_\alpha}{\sqrt{c_\alpha^2 + \rho_c^2}} + \dfrac{c_\beta}{\sqrt{c_\beta^2 + \rho_c^2}}}{\rho_c} \right] \frac{\vec{a} \times \vec{b}}{|\vec{a} \times \vec{b}|}$$

where $\qquad c_\alpha = |\vec{a}| \cos\alpha = \dfrac{(-\vec{a}) \cdot (-\vec{c})}{|\vec{c}|}$

and $\qquad c_\beta = |\vec{b}| \cos\beta = \dfrac{(-\vec{b}) \cdot \vec{c}}{|\vec{c}|}$.

The induced velocity ($\vec{q}$) at a point inside the core can then be written, assuming solid body rotation of the vortex core:

$$\vec{q} = \left[\frac{|(-\vec{c}) \times (-\vec{a})|}{|\vec{c}|\ \rho_c} \right] \vec{q}_{\rho_c}$$

As mentioned in the Vortex Wake Model section, the trailing vortex segments $\Delta\phi$ on either side of point P_η are considered separately from the rest of the wake to include accurately the effects of vortex core size. Reference 9 gives an expression for the induced velocity, due to a circular arc vortex segment with

34

a finite core radius ($\rho_c R$) and $\rho_c \ll 1$, at one end of the vortex arc. Put into our notation, this gives an expression for $\vec{q}_t$ when $\zeta = 0$, $\ell = 1.0$, and $\phi = \psi + \zeta$ or $\psi + \zeta + \Delta\phi$:

$$\vec{q}_t = \frac{1}{2}\left\{ \ln\left[8\left(\frac{\rho}{\rho_c}\right) \tan\left(\frac{\Delta\phi}{4}\right)\right] + \frac{1}{4} \right\} \left(\frac{\vec{c}_1 \times \vec{c}_2}{|\vec{c}_1 \times \vec{c}_2|} \right)$$

where $\vec{c}_1 = \vec{c}_t(1.0, \psi + \zeta + \Delta\phi)$, $\vec{c}_2 = \vec{c}_t(1.0, \psi + \zeta)$,

$$\rho = \left(\frac{|\vec{c}_1|}{2\cos\upsilon} \right), \quad \upsilon = \tan^{-1}\left[\frac{|\vec{c}_2|^2 - \vec{c}_1 \cdot (-\vec{c}_2)}{|\vec{c}_1 \times (-\vec{c}_2)|} \right] \quad \left(0 \le \upsilon \le \frac{\pi}{2} \right)$$

As shown in Fig. A4, the radius of curvature (ρ) used is that for a circular arc passed through the three end points (one of which is common) of $\vec{c}_1$ and $\vec{c}_2$

When $\zeta = 0$ and $\phi = \psi + \zeta$ point P_η is located on a shed or bound vortex segment and since a straight line vortex induces no velocity on itself $\vec{q}_s = 0$.

The key approximations used here to obtain more rapid computer solutions are those involved in the specification of $\vec{D2}$ and $\vec{D3}$ the distortion of points P_ℓ and P_η, respectively. When the rigid wake approximation is used, this is straightforward. At time t_d point P_ℓ is located, using the rigid wake approximation:

$$DI2 = DJ2 = 0, \quad DK2 = \left[\frac{C_T}{2\sqrt{\mu^2 + \lambda^2}} \right] (\phi' - \phi),$$

where

$$\lambda = -\mu \tan i + \left[\frac{C_T}{2\sqrt{\mu^2 + \lambda^2}} \right]$$

is the nondimensional, uniform inflow velocity, perpendicular to the TPP, from momentum theory and C_T is the thrust coefficient of the rotor. At time t_d point P_η is located using the rigid

35

wake approximation:

$$DI3 = DJ3 = 0, \quad DK3 = \left[\frac{C_T}{2\sqrt{\mu^2 + \lambda^2}}\right](\phi' - \psi - 5)$$

It may be helpful here to recall that:

$$t_d - t_\ell = (\phi' - \phi)/\Omega$$

and

$$t_d - t_\eta = (\phi' - \psi - 5)/\Omega$$

The method of determining $\vec{D2}$ and $\vec{D3}$ for the general case when a nonrigid wake approximation may be used is best illustrated by an outline of the important steps in the wake distortion computation.

1) Input the data including $\vec{D'}$, which is the distortion ($\vec{D}$) output by the previous iteration. For the first iteration, the rigid wake approximation is used to define $\vec{D'}$:

$$DI' = DJ' = 0, \quad DK' = \left[\frac{C_T}{2\sqrt{\mu^2 + \lambda^2}}\right]\Omega \Delta t$$

where Δt is the time elapsed since the element of vorticity whose distortion is to be approximated by $\vec{D'}$ was trailed from the rotor blade.

2) Define $\vec{D''}$ as the distortion used to determine the wake geometry used for induced velocity calculations. Initially set $\vec{D''} = \vec{D'}$.

3) Set a counter $n = 1$

4) Compute $\vec{D}(\psi, \phi' - \psi - 5)$ for $\quad 0 \leq \psi \leq 2\pi$
and $(n-1)n_1 \Delta\phi \leq (\phi' - \psi - 5) \leq n n_1 \Delta\phi$
During this calculation $\vec{D''}$ remains unchanged which implies that $\vec{q}(\ell, 5, \psi, \phi)$ for any given $\ell, 5, \psi, \phi$ combination will remain unchanged for all values of ϕ' such that $(n-1)n_1 \Delta\phi \leq (\phi' - \psi - 5) \leq n n_1 \Delta\phi$.

36

This means that:

$$\vec{Q}(\ell, s, \psi, \phi'') = \vec{Q}(\ell, s, \psi, \phi'' - \Delta\phi) + \vec{q}(\ell, s, \psi, \phi'')$$

and:

$$\vec{D}(\psi, \phi' - \psi - s) = \vec{D}(\psi, \phi' - \psi - s - \Delta\phi) + \vec{\Delta D}(s, \psi, \phi')$$

Which avoids recomputing all of the $\vec{q}(\ell, s, \psi, \phi)$ and summing to get $\vec{Q}(\ell, s, \psi, \phi'')$ and $\vec{D}(\psi, \phi' - \psi - s)$ for each different ϕ'.

5) Now update $\vec{D''}$. Let $\vec{D''}(\psi, \phi' - \psi - s) = \vec{D}(\psi, \phi' - \psi - s)$ for $0 \le \psi \le 2\pi$ and $(n-1)n_1 \Delta\phi \le (\phi' - \psi - s) \le n n_1 \Delta\phi$.

6) If $n n_1 \Delta\phi \ge 2\pi m$ end of iteration, otherwise continued.

7) $n = n + 1$ go to step 4. Now because $\vec{D''}$ was changed in step 5, all of the $\vec{q}(\ell, s, \psi, \phi)$ will have to be recomputed in step 4. However, they need only be computed once for each time step 4 is reached (see the explanation of this under step 4). From this description, it can be seen that n_1, which determines how often $\vec{D''}$ is updated, should be as large as possible (without compromising convergence) to minimize the number of times $\vec{q}$ must be recomputed.

Now $\vec{D2}$ and $\vec{D3}$ can be computed. For locating point P_ℓ when $\ell = 0.5$, the rigid wake approximation is always used. For locating point P_ℓ when $\ell = 1.0$ and for locating point P_n at all times $\vec{D2}$ and $\vec{D3}$ are calculated in terms of the $\vec{D'}$ and $\vec{D''}$ defined above. For $\phi' - \phi \le (n-1)n_1 \Delta\phi$, $\vec{D''}$ is equal to $\vec{D}$ and should be a better approximation to the distortion than $\vec{D'}$ from the previous iteration, therefore:

$$\vec{D2} = \vec{D''}(\phi, \phi' - \phi) \quad \text{for} \quad \phi' - \phi \le (n-1)n_1 \Delta\phi .$$

For $(n-1)n_1 \Delta\phi \le \phi' - \phi \le 2\pi m$, $\vec{D''}$ is still equal to $\vec{D'}$. A better approximation to the distortion in this range than just using $\vec{D'}$ is to use $\vec{D''}$ for the distortion accumulated in the initial $\dfrac{(n-1)n_1 \Delta\phi}{\Omega}$ time interval and add the $\vec{D'}$ distortion

accumulated in the last $\dfrac{\phi'-\phi-(n-1)n_1\Delta\phi}{\Omega}$ time interval; therefore:

$$\vec{D2} = \vec{D}''(\phi,(n-1)n_1\Delta\phi) + \vec{D}'(\phi,\phi'-\phi) - \vec{D}'(\phi,(n-1)n_1\Delta\phi)$$

for $(n-1)n_1\Delta\phi < \phi'-\phi \le 2\pi m$.

For $2\pi m < \phi'-\phi$, the distortion is not calculated. The distortion for this range is approximated by using the definition above for the distortion accumulated in the initial $2\pi m/\Omega$ time interval and the rigid wake approximation for the distortion thereafter. Therefore,

$$DI2(\phi,\phi'-\phi) = DI2(\phi,2\pi m)$$

$$DJ2(\phi,\phi'-\phi) = DJ2(\phi,2\pi m)$$

$$DK2(\phi,\phi'-\phi) = DK2(\phi,2\pi m) + (\phi'-2\pi m-\phi)\left[\frac{C_T}{2\sqrt{\mu^2+\lambda^2}}\right]$$

for $2\pi m < \phi'-\phi$.

Since $(n-1)n_1\Delta\phi \le (\phi'-\psi-s) \le nn_1\Delta\phi$, $\vec{D3}$ is defined in a fashion similar to $\vec{D2}$ in this range:

$$\vec{D3} = \vec{D}''(\psi,(n-1)n_1\Delta\phi) + \vec{D}'(\psi,\phi'-\psi-s) - \vec{D}'(\psi,(n-1)n_1\Delta\phi).$$

A few auxiliary calculations are needed to find some of the inputs for the computational procedure outlined above. The thrust coefficient (C_T) is defined conventionally,

$$C_T = \frac{T}{\rho\pi R^2(\Omega R)^2}$$

38

where the thrust $T = \sqrt{W^2 + D^2}$, ρ is the atmospheric density, W is the weight of the aircraft and D is the drag. The tip path plane incidence (i) can be estimated by: tan i $\simeq (D/W)$, especially for low μ where wake distortion is most important. The coning angle (a_o) can be estimated from uniform inflow theory or from a rigid wake airload calculation.

The time average, nondimensional, bound circulation (γ_o) is found by requiring that the proper thrust (or C_T) is developed. The lift per unit span is $L = \rho V \Gamma$. The thrust is

$$T = \frac{1}{2\pi} \int_0^{2\pi} \int_0^1 n_b R L \, d\eta \, d\psi \, ,$$

where n_b = number of blades. In terms of time average values:

$$L_o = \rho V_o \Gamma_o \qquad \text{and} \qquad T = \int_0^1 n_b R L_o \, d\eta$$

where

$$V_o = \eta \Omega R \qquad \text{and} \qquad \Gamma_o = 2\pi b \Omega R Y_o$$

Recalling the definitions of C_T and σ, and the approximation that there is constant circulation between $\eta = \ell_I$ (normally 0.5) and 1.0 and zero circulation inboard:

$$\sigma = \frac{n_b 2 b R}{\pi R^2} = \left(\frac{\text{blade area}}{\text{disk area}} \right)$$

$$C_T = \int_{\ell_I}^{1.0} \frac{\rho n_b R \, 2\pi b \, \Omega R Y_o \, \eta \, \Omega R}{\rho \pi R^2 (\Omega R)^2} \, d\eta = \frac{\sigma \pi Y_o}{2} \left(1 - \ell_I^2 \right)$$

$$\therefore Y_o = \frac{2 C_T}{\pi \sigma \left(1 - \ell_I^2 \right)}$$

39

A first estimate of the circulation of the vortex wake neglects the higher harmonics and takes the time average (zeroth harmonic) bound circulation (Γ_o) as the circulation of the trailing wake. This implies γ_t = 1.0 and, conserving circulation, γ_s = 0.0.

An improved estimate of the vortex wake circulation can be obtained from a time history of angle of attack (α) as calculated by an airload calculation (either uniform inflow, rigid wake, or the wake geometry from a previous iteration may be used in this airload calculation). The angle of attack $\alpha(\psi,\eta)$ is computed both as a function of azimuth angle ψ (time) and radial station η. The lift per unit span is $L = \rho V \Gamma$ or alternately,

$$L = \frac{1}{2}\rho V^2 2b \, C_L \quad \text{and} \quad C_L = \alpha \frac{\partial C_L}{\partial \alpha} = \alpha a \quad .$$

Since
$$V = \Omega R (\eta + \mu \sin \psi) \quad \text{and} \quad \Gamma = 2\pi b \Omega R \gamma \quad ,$$
$$L = \rho \Omega R (\eta + \mu \sin \psi) \, 2\pi b \Omega R \gamma$$
and
$$L = \rho a b (\Omega R)^2 (\eta + \mu \sin \psi)^2 \alpha \quad .$$

The thrust of a given blade as a function of azimuth is
$$T_b = \int_{\eta_o}^{1} L R \, d\eta \quad ,$$
where η_o is the nondimensional root cutout. Requiring the $T_b(\psi)$ developed by the model used here, which assumes $\gamma(\psi)$ is constant from $\eta = \ell_I$ (normally 0.5) to $\eta = 1.0$ (the blade tip) and zero inboard be equal to the $T_b(\psi)$ computed by the airloads calculation:

$$\int_{\eta_o}^{1} \rho a b (\Omega R)^2 (\eta + \mu \sin \psi)^2 \alpha \, d\eta = \int_{\ell_I}^{1} \rho \, 2\pi b R (\Omega R)^2 (\eta + \mu \sin \psi) \gamma \, d\eta$$

$$\gamma(\psi) \int_{\ell_I}^{1} (\eta + \mu \sin \psi) \, d\eta = \frac{a}{2\pi} \int_{\eta_o}^{1} (\eta + \mu \sin \psi)^2 \alpha(\psi,\eta) \, d\eta$$

40

$$\int_{l_I}^{1} (\eta + \mu \sin \psi)\, d\eta = \left(\frac{1 - l_I^2}{2}\right) + \left(1 - l_I\right)\mu \sin \psi$$

Recalling that γ_t is normalized by γ_o:

$$\gamma_t(1.0, \psi) = \left(\frac{a}{2\pi \gamma_o}\right)\left\{\frac{\int_{\eta_o}^{1}(\eta + \mu \sin \psi)^2 \, \alpha(\psi, \eta)\, d\eta}{\left[\frac{1}{2}(1 - l_I^2) + (1 - l_I)\mu \sin \psi\right]}\right\}$$

Then $\gamma_t(l_I, \phi) = -\gamma_t(1.0, \phi)$ and conserving circulation,

$$\gamma_s(\phi) = \gamma_t(1.0, \phi + \Delta\phi) - \gamma_t(1.0, \phi)\ .$$
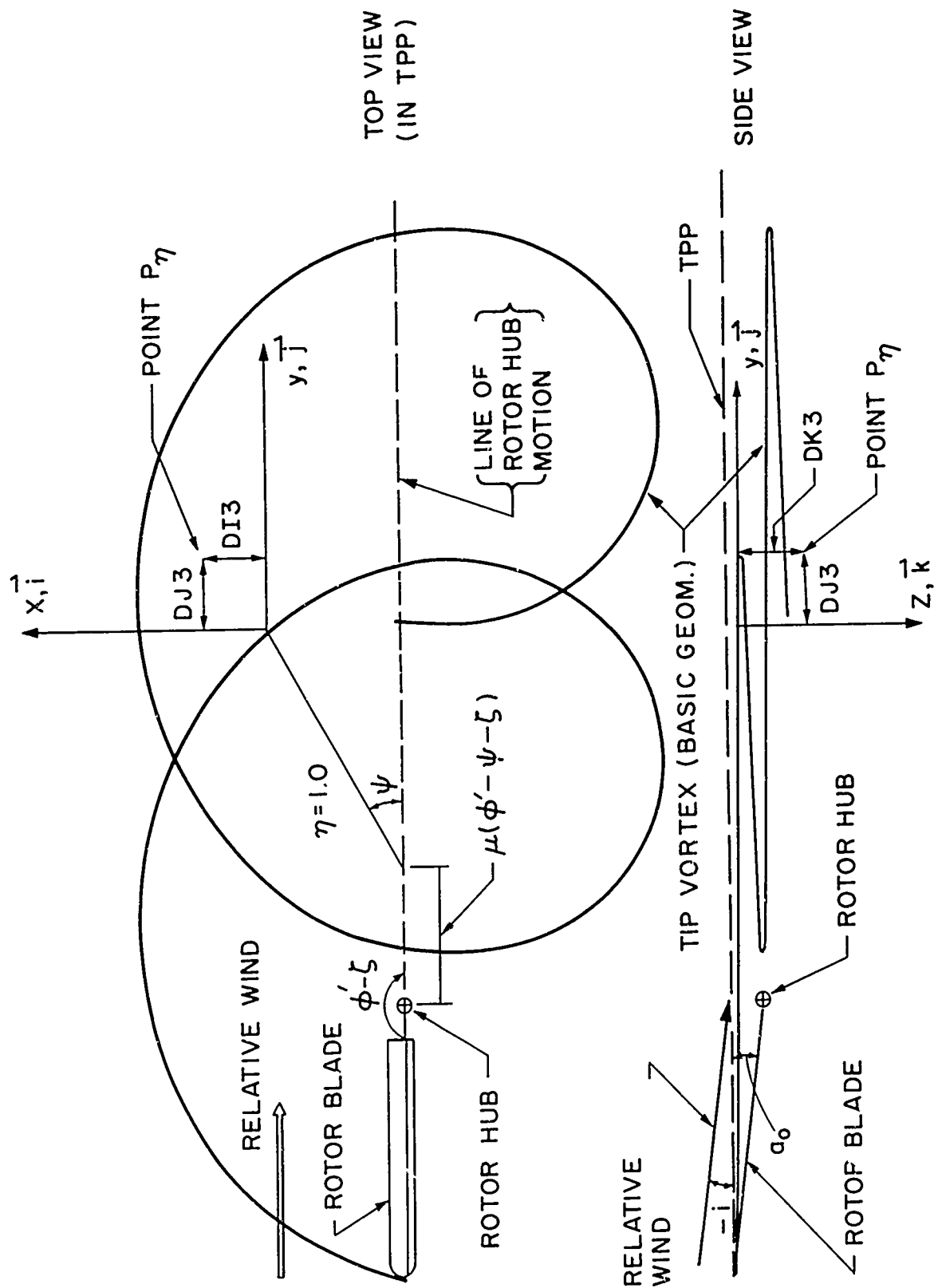
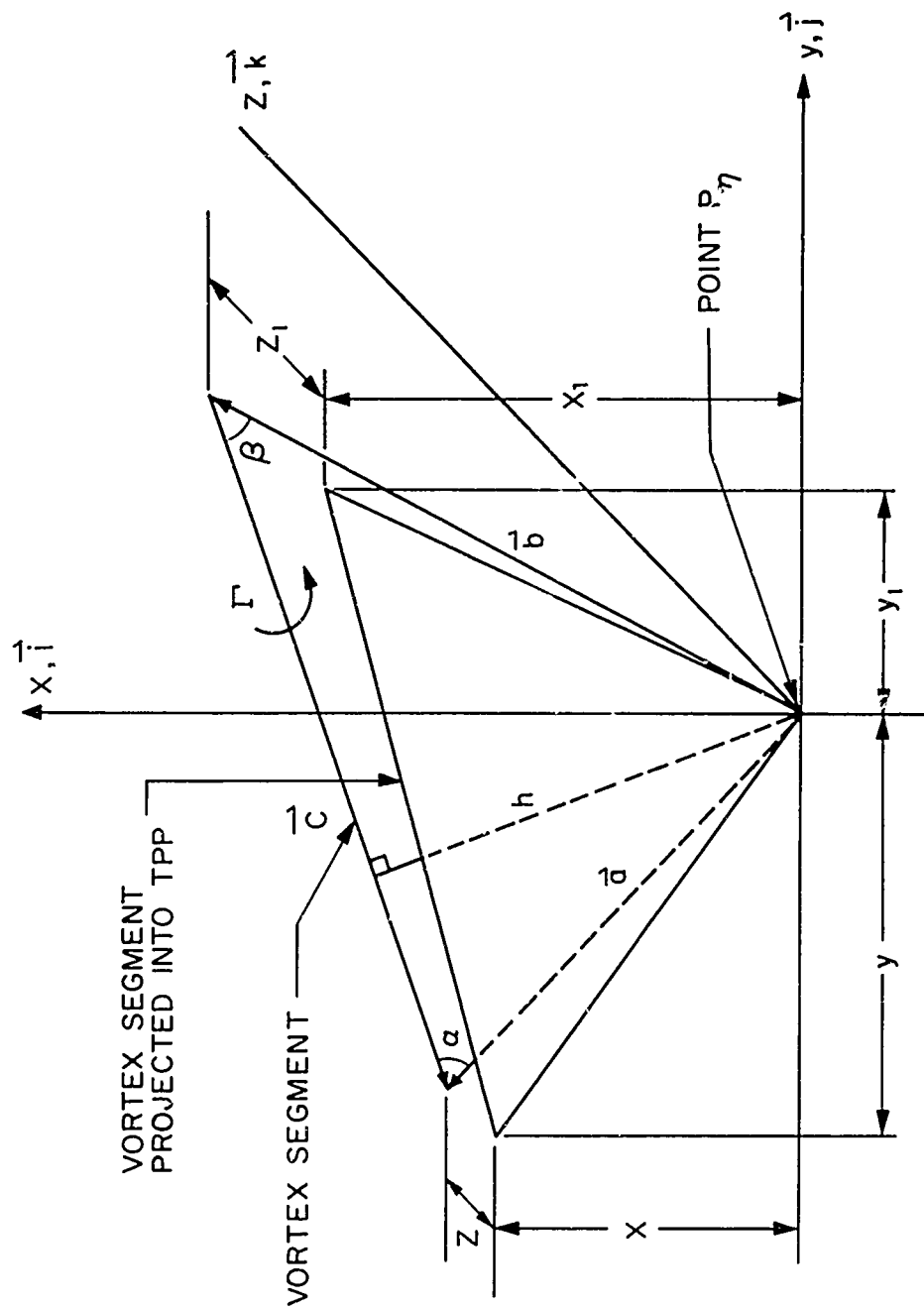FIGURE AI: TIP VORTEX BASIC GEOMETRY ($\zeta = 0$ CASE)
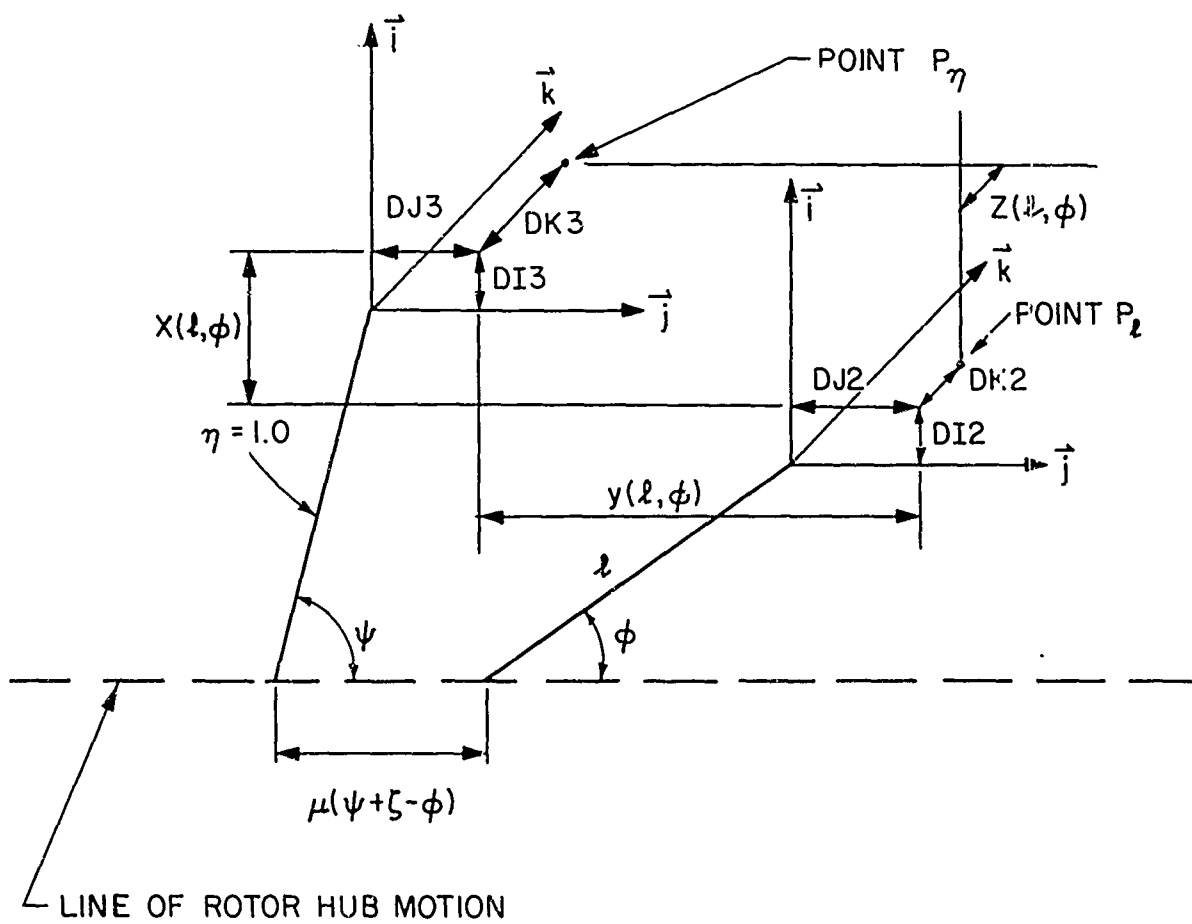
42

FIG. A2 VORTEX SEGMENT GEOMETRY
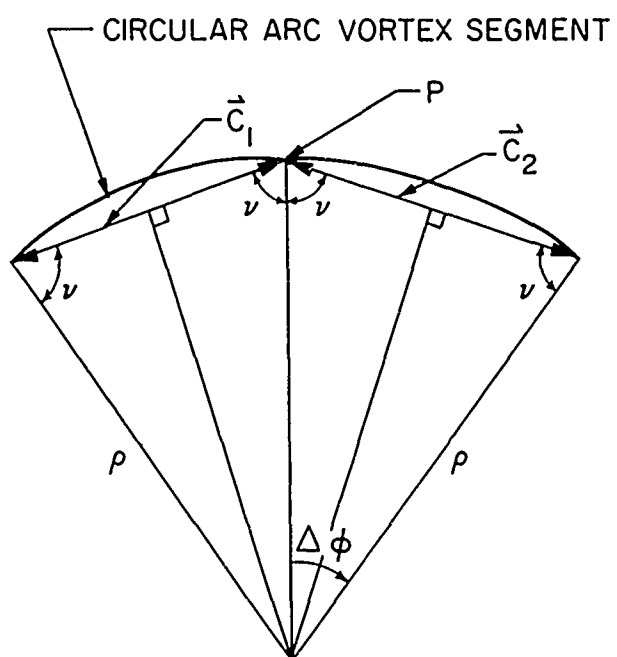
FIGURE A3: LOCATION OF P_{ℓ} RELATIVE TO P_{η}

FIGURE A4 : CIRCULAR ARC VORTEX SEGMENT GEOMETRY

DOCUMENT CONTROL DATA - R & D

Security classification of title, body of abstract and indexing annotation must be entered when the overall report is classified)

1 ORIGINATING ACTIVITY (Corporate author)	2a. REPORT SECURITY CLASSIFICATION
Massachusetts Institute of Technology Aeroelastic and Structures Research Lab. Cambridge, Massachusetts	UNCLASSIFIED
	2b GROUP

1 REPORT TITLE

A METHOD OF COMPUTING HELICOPTER VORTEX WAKE DISTORTION

4 DESCRIPTIVE NOTES (Type of report and inclusive dates)

Technical report

5 AUTHOR(S) (First name, middle initial, last name)

Michael P. Scully

6 REPORT DATE	7a. TOTAL NO OF PAGES	7b. NO OF REFS
June 1967	52	11

8a CONTRACT OR GRANT NO	9a. ORIGINATOR'S REPORT NUMBER(S)
NOw 66-0286-d	
b PROJECT NO	ASRL 138-1
	9b OTHER REPORT NO(S) (Any other numbers that may be assigned this report)
d	

10 DISTRIBUTION STATEMENT

Distribution of this report is unlimited

11 SUPPLEMENTARY NOTES	12 SPONSORING MILITARY ACTIVITY
	Department of the Navy, Naval Air Systems Command, Airframes Div. Washington, D.C. 20360

13 ABSTRACT

A method for computing the geometry of the tip vortex of a helicopter rotor in steady, forward flight, including the distortion due to the velocities induced by the vortex wake, has been developed. The relative importance of various parameters and approximations used by this method has been evaluated for one test case, including comparison with experimental results obtained from a flow visualization study.

KEY WORDS	LINK A		LINK B		LINK C	
	ROLE	WT	ROLE	WT	ROLE	WT
Rotor Aerodynamics						
Vortex Wake Geometry						
Unsteady Aerodynamics						